

Supplemental Information Section

## **Isolation and characterization of the $[\text{Ga}_2\text{Al}_{18}\text{O}_8(\text{OH})_{36}(\text{H}_2\text{O})_{12}]^{8+}$ cluster: Cationic Variations on the Wells-Dawson topology**

**M. Fairley, K. W. Corum, A. Johns, M. Basile, J. de Groot, D. K. Unruh, S. E. Mason\*, and T. Z. Forbes\***

Department of Chemistry, University of Iowa, Iowa City, IA 52242

\*Corresponding authors: [tori-forbes@uiowa.edu](mailto:tori-forbes@uiowa.edu), [sara-mason@uiowa.edu](mailto:sara-mason@uiowa.edu)

### **Additional Synthesis Information**

The reagents  $\text{AlCl}_3 \cdot 6\text{H}_2\text{O}$  (Fisher Scientific), NaOH (Fisher Scientific),  $\text{GaCl}_3$  (Fisher Scientific) and 2,7-naphthalene disulfonic acid disodium salt (97%, Sigma Aldrich) were used as received and all solutions were prepared using distilled water as the solvent. A partially hydrolyzed aluminum stock solution was prepared by heating 25 mL of 0.25 M  $\text{AlCl}_3$  (6.25 mmol) solution to 80 °C in a water bath, followed by a drop wise addition of 60 mL of 0.25 M NaOH (6.25 mmol) to a hydrolysis ratio ( $\text{OH}^- / \text{Al}^{3+}$ ) of 2.4. After cooling to room temperature, 7 mL of the clear aluminum stock solution and one mL of a 0.25 M solution of  $\text{GaCl}_3$  were loaded in to a 23 mL Teflon-lined Parr reaction vessel. The solution was heated in a gravimetric oven at 80 °C for 24 hours and allowed to cool to room temperature. A 4 mL aliquot of the resulting solution was added to a glass scintillation vial with 1.5 mL of a 0.1 M 2,7-naphthalene disulfonate solution as the crystallization agent. After three weeks of slow evaporation, an amorphous flocculant formed alongside clear blocky crystals of  $\text{Ga}_2\text{Al}_{18}$  with approximate yields of 30% for the crystalline material based upon Al.

## **Single-crystal X-ray Diffraction**

Crystals were removed from the mother liquor, coated in Infinium oil, and mounted on a Nonius Kappa CCD single crystal X-ray diffractometer equipped with MoK $\alpha$  radiation ( $\lambda = 0.7107 \text{ \AA}$ ) and a low temperature cryostat. Data collection was carried out by Collect,<sup>14</sup> while cell refinement and data reduction were handled by APEX II software and a semi-empirical absorption correction was applied by SADABS.<sup>15</sup> The structures were solved using direct methods and refined on the basis of  $F^2$  for all unique data using the Bruker SHELXTL Version 5 system of programs.<sup>16</sup> The Al, Ga, and S atoms were located in the direct methods solutions and the O and C atoms were identified in the difference Fourier maps calculated following refinement of the partial-structure models. The cluster crystallizes in a triclinic space group,  $P-1$ , with  $a = 10.0721(7) \text{ \AA}$ ,  $b = 16.7628(11) \text{ \AA}$ ,  $c = 17.7945(12) \text{ \AA}$ ,  $\alpha = 90.852(2)^\circ$ ,  $\beta = 99.861(2)^\circ$ ,  $\gamma = 101.175(2)^\circ$ . Hydrogen atom positions for the naphthalene groups were placed using a riding model, but additional hydrogen atoms were not located on the interstitial water molecules or the Ga<sub>2</sub>Al<sub>18</sub> cluster due to disorder of solvent in the void space. The extended crystallographic packing for the solid material is shown in Figure S1.

**Table S1.** Selected bond distances and angles for **Ga<sub>2</sub>Al<sub>18</sub>**

Ga(1)-O(4)	1.858(3)	Al(7)-O(22)	1.828(3)
Ga(1)-O(2)	1.889(3)	Al(7)-O(24)	1.863(3)
Ga(1)-O(14)	1.895(3)	Al(7)-O(7)	1.865(3)
Ga(1)-O(1)	1.898(3)	Al(7)-O(16)	1.871(3)
		Al(7)-O(23)	1.911(3)
Al(1)-O(9)	1.828(3)	Al(7)-O(4) <sup>a</sup>	2.024(3)
Al(1)-O(19)	1.852(3)		
Al(1)-O(3)	1.900(3)	Al(8)-O(25)	1.834(3)
Al(1)-O(15)	1.901(3)	Al(8)-O(22)	1.834(3)
Al(1)-O(11)	1.922(3)	Al(8)-O(8)	1.869(3)
Al(1)-O(1) <sup>a</sup>	2.030(3)	Al(8)-O(27)	1.883(3)
		Al(8)-O(17)	1.901(3)
Al(2)-O(25)	1.840(3)	Al(8)-O(4) <sup>a</sup>	2.025(3)
Al(2)-O(27)	1.855(3)		
Al(2)-O(26) <sup>a</sup>	1.885(3)	Al(9)-O(19)	1.833(3)
Al(2)-O(21)	1.894(3)	Al(9)-O(13)	1.848(3)
Al(2)-O(10)	1.900(3)	Al(9)-O(6)	1.852(3)
Al(2)-O(14) <sup>a</sup>	2.060(3)	Al(9)-O(26)	1.876(3)
		Al(9)-O(14)	1.981(3)
Al(3)-O(7)	1.844(3)	Al(9)-O(1) <sup>a</sup>	1.992(3)
Al(3)-O(24)	1.851(3)		
Al(3)-O(12) <sup>a</sup>	1.883(3)	S(1)-O(34)	1.447(4)
Al(3)-O(18)	1.896(3)	S(1)-O(29)	1.452(3)
Al(3)-O(28)	1.901(3)	S(1)-O(37)	1.456(4)
Al(3)-O(2) <sup>a</sup>	2.087(3)	S(1)-C(5)	1.771(5)
Al(4)-O(13)	1.840(3)	S(2)-O(38)	1.455(3)
Al(4)-O(5)	1.861(3)	S(2)-O(33)	1.455(4)
Al(4)-O(18)	1.876(3)	S(2)-O(35)	1.455(3)
Al(4)-O(10) <sup>a</sup>	1.884(3)	S(2)-C(13)	1.772(5)
Al(4)-O(14)	1.936(3)		
Al(4)-O(2) <sup>a</sup>	1.951(3)	S(3)-O(32)	1.451(3)
		S(3)-O(31)	1.451(3)
Al(5)-O(9)	1.836(3)	S(3)-O(30)	1.459(3)
Al(5)-O(16)	1.849(3)	S(3)-C(4)	1.761(5)
Al(5)-O(8)	1.881(3)		
Al(5)-O(20)	1.905(3)	S(4)-O(36)	1.448(4)
Al(5)-O(11)	1.918(3)	S(4)-O(40)	1.454(5)
Al(5)-O(4) <sup>a</sup>	1.979(3)	S(4)-O(39)	1.455(4)
		S(4)-C(14)	1.770(5)
Al(6)-O(6)	1.844(3)		
Al(6)-O(5) <sup>a</sup>	1.858(3)		
Al(6)-O(15)	1.880(3)		
Al(6)-O(12)	1.883(3)		
Al(6)-O(2)	1.950(3)		
Al(6)-O(1) <sup>a</sup>	1.965(3)		

a: -x+2,-y+2,-z+1.

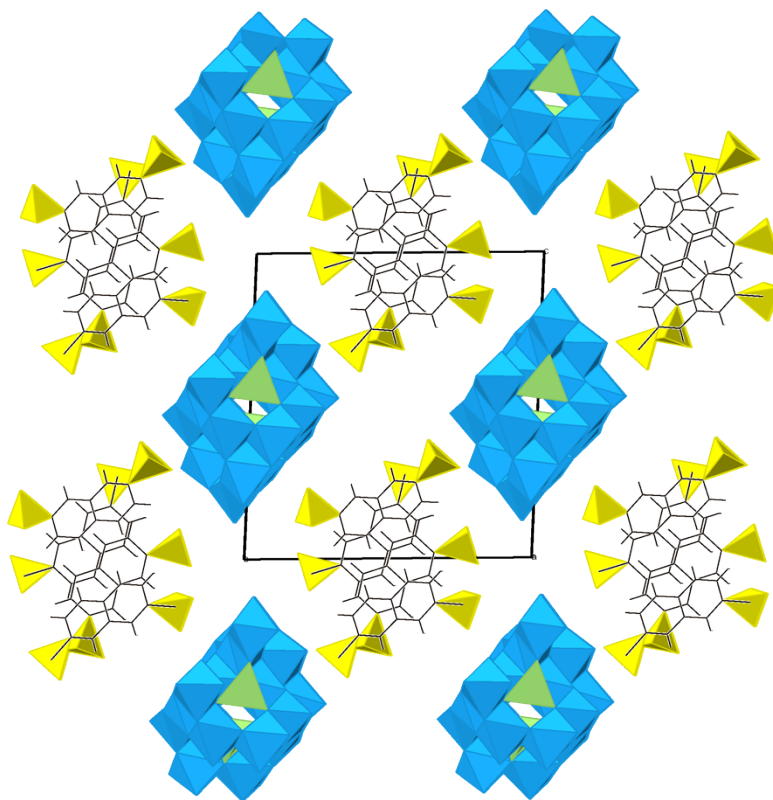


**Figure S1.** The extended crystallographic lattice for the  $\text{Ga}_2\text{Al}_{18}$  compound. Ga, Al, and S are represented by green, blue, and yellow polyhedra, respectively. Wire frame is used to depict the C in the naphthalene rings and the H and O atoms are not shown for clarity.

### **Bond Valence Analysis**

Bond Valence analysis parameters calculations were performed based upon methods reported by Brese and O'Keefe,<sup>17</sup> to confirm the overall charge and protonation of the cluster. Bond valence sums ( $v_{ij}$ ) are calculated using the following formula, utilizing the bond distance obtained from the crystallographic data ( $d_{ij}$ ):

$$v_{ij} = \exp\left[\frac{R_{ij} - d_{ij}}{b}\right]$$

The  $R_{ij}$  values for Al(III) and Ga(III) were 1.620 and 1.730, respectively, while the b parameter was 0.37 for both cations.<sup>17</sup>

**Table S2.** Bond valence of the  $\text{Ga}_2\text{Al}_{18}$  cluster indicate that the overall structure is  $[\text{Ga}_2\text{Al}_{18}\text{O}_8(\text{OH})_{36}(\text{H}_2\text{O})_{12}]^{8+}$ .

	Ga1	Al1	Al2	Al3	Al4	Al5	Al6	Al7	Al8	Al9	Sum	Ligand
O1	0.635	0.330					0.394			0.366	1.725	O
O2	0.708			0.283	0.409		0.410				1.809	O
O3		0.469									0.469	H <sub>2</sub> O
O4	0.708					0.379		0.336	0.335		1.757	O
O5					0.521		0.526				1.047	OH
O6							0.546			0.534	1.080	OH
O7				0.546				0.516			1.062	OH
O8						0.494			0.510		1.004	OH
O9		0.570				0.558					1.128	OH
O10			0.469		0.490						0.959	OH
O11		0.442				0.447					0.889	OH
O12				0.491			0.491				0.982	OH
O13					0.552					0.540	1.092	OH
O14	0.640		0.304		0.426					0.377	1.747	O
O15		0.468					0.495				0.963	OH
O16						0.539		0.507			1.046	OH
O17									0.468		0.468	H <sub>2</sub> O
O18				0.474	0.501						0.975	OH
O19		0.534								0.562	1.097	OH
O20						0.463					0.463	H <sub>2</sub> O
O21			0.477								0.477	H <sub>2</sub> O
O22								0.570	0.561		1.131	OH
O23								0.455			0.455	H <sub>2</sub> O
O24				0.536				0.519			1.054	OH
O25			0.552						0.561		1.113	OH
O26			0.489							0.501	0.989	OH
O27			0.530						0.491		1.021	OH
O28				0.468							0.468	H <sub>2</sub> O
<b>B.V.</b>	<b>2.6904</b>	<b>2.8135</b>	<b>2.8208</b>	<b>2.7980</b>	<b>2.8981</b>	<b>2.8790</b>	<b>2.8614</b>	<b>2.9027</b>	<b>2.9256</b>	<b>2.8799</b>		
<b>IDEAL</b>	<b>3</b>											

## Elemental Analysis

$\text{Ga}_2\text{Al}_{18}$  was characterized by a Varian 720-ES ICP-OES instrument to determine the presence of Ga within the material. A small quantity (5 mg) of the characterized powder was dissolved in a 2% nitric acid solution in triplicate. A standard curve was created in a similar matrix using a 1000 ppm Ga standard purchase from Fisher Scientific. The experiment was performed on a Varian ICP-OES 720 system using the 287.4, 294.4, and 417.2 nm spectral emissions. Ga concentrations were measured at 12.2, 14.2, and 11.6 ppm within these samples.

## $^{71}\text{Ga}$ NMR Spectroscopy

$^{71}\text{Ga}$  NMR spectroscopy was performed on the solution that resulted in the crystallization of the  $\text{Ga}_2\text{Al}_{18}$  cluster. As described above, 7 mL of  $\text{Al}_{13}$  solution was mixed with 1.0 mL 0.25 M  $\text{GaCl}_3$  inside a Teflon liner, which was placed inside a Parr acid digestion vessel and heated under static pressure at 80 C for 48 hours in the oven, where it was allowed to gradually cool. An 800  $\mu\text{L}$  aliquot of  $\text{D}_2\text{O}$  was mixed with the original solution and then a 600  $\mu\text{L}$  sample was placed into a glass NMR tube. Solution gallium-71 NMR spectrum was acquired on Bruker DRX-400 ( $B_0 = 9.40$  T) NMR instrument using standard 5 mm BBO probe at room temperature. The sample was dissolved in 90%  $\text{H}_2\text{O}$  and 10%  $\text{D}_2\text{O}$ . One dimension direct observing pulse sequence was applied. The Ga-71 NMR spectrum of the hydrolyzed solution is the sum of 200k scans with relaxation delay of 0.2 s. Gallium NMR chemical shifts were referenced with respect to an external solution of 1.0 M  $\text{Ga}(\text{NO}_3)_3$ .<sup>18</sup>

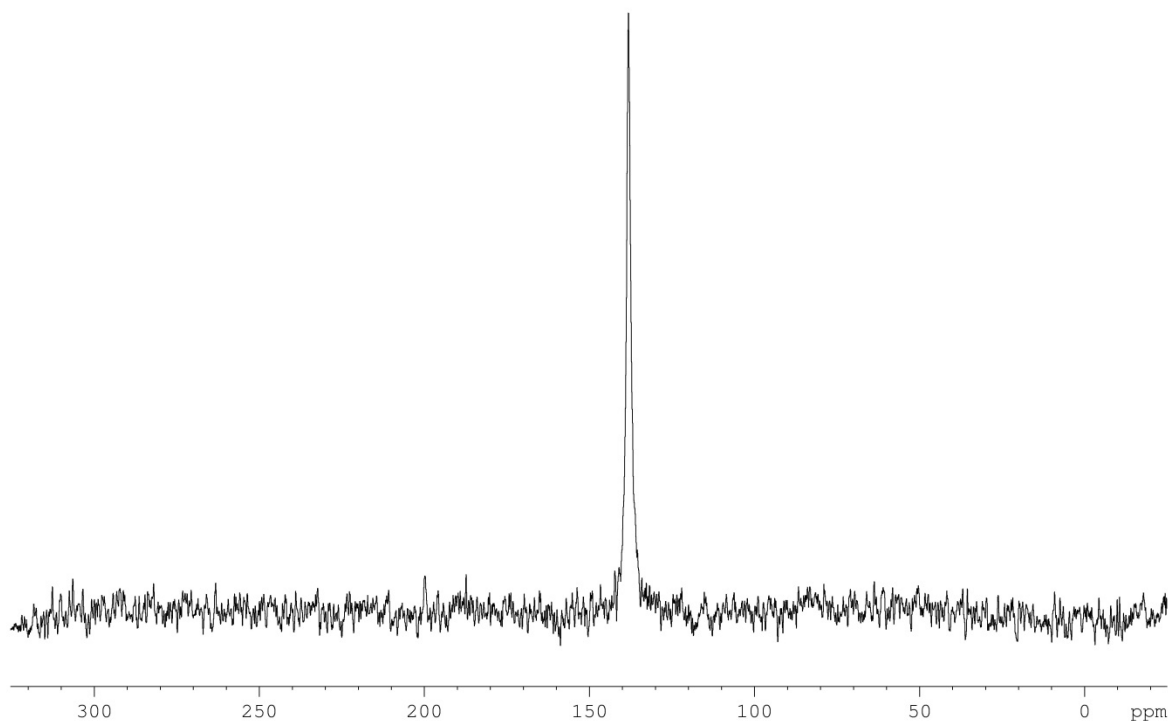


**Figure S2.**  $^{71}\text{Ga}$  NMR of the hydrolyzed solution that resulted in the formation of the  $\text{Ga}_2\text{Al}_{18}$  cluster.

Octahedrally coordinated Ga(III) is distinguished by a broad peak that is centered around 0 ppm, whereas a sharper downfield peak is observed with Ga(III) in tetrahedral coordination. Only tetrahedrally coordinated Ga(III) was observed in the solution that produced the  $\text{Ga}_2\text{Al}_{18}$  cluster and the peak was observed at 138.14 ppm. Previous NMR data of the  $\epsilon\text{-GaAl}_{12}$  cluster reported the tetrahedral shift at 137.8 ppm, which is not significantly different than observed in the mother liquor.<sup>19</sup> However, it is important to note that the initial solution contained preformed  $\epsilon\text{-Al}_{13}$  clusters with added Ga(III) halide salt and synthetic method is different than the previously reported protocol for the formation of  $\epsilon\text{-GaAl}_{12}$ , which utilized hydrolysis of  $\text{AlCl}_3$  and  $\text{GaCl}_3$  salts.<sup>7</sup> In addition, the similarity in the chemical environment around  $\epsilon\text{-GaAl}_{12}$  and  $\text{Ga}_2\text{Al}_{18}$  may result in only minor shifts in the spectra. This scenario is observed in Al(III)

Keggin structures where the observed shifts for the  $\epsilon$ -Al<sub>13</sub>,  $\epsilon$ -Al<sub>13</sub>, Al<sub>26</sub>, and Al<sub>30</sub> clusters are located at 62.9, 64.5, and 66.3, and 71 ppm, respectively.<sup>6a, 20, 21, 22</sup> Alternatively, the **Ga<sub>2</sub>Al<sub>18</sub>** cluster may be a minor species in initial hydrolyzed solution and cannot be detected using NMR spectroscopy. Additional experiments are currently being performed to provide more insight into the NMR spectra of the hydrolyzed Ga/Al system.

### **Electrospray Ionization Mass Spectroscopy**

The presence of the mixed Ga/Al cluster was examined by electrospray ionization mass spectrometry (ESI-MS), as anions in an aqueous matrix. Mass spectra were collected on a ThermoElectron LCQ Deca Quadrupole Ion-Trap Mass Spectrometer operated in positive ion mode. Electrospray conditions were maintained throughout the experiment. Samples were flowed via direct infusion with a 250  $\mu$ L Hamiltonian glass syringe at a flow rate of 30  $\mu$ L min<sup>-1</sup> using nitrogen as the nebulizing gas. The capillary temperature within the ESI source was set at 112 °C to promote effective dissolution and a capillary voltage of +14 kV was used throughout the experimental trials. Additional programmable ESI parameters were set as follows: ionization spray voltage, +4.5 kV; tube lens offset voltage, -10 V. Fragmentation of the molecular species present in the solid state compounds were investigated by dissolving a small amount of the Ga<sub>2</sub>Al<sub>18</sub> crystallites in an aqueous solution. In addition, the hydrolyzed solution that resulted in the formation of the Ga<sub>2</sub>Al<sub>18</sub> cluster was also analyzed to investigate the prevalence of the clusters in solution.

The **Ga<sub>2</sub>Al<sub>18</sub>** clusters were not stable upon dissolution and ionization within the MS (Fig. S3), but fragments could be identified in the spectrum (Table S3). Based upon the isotope splitting the presence of chlorine could be observed, which is likely due to the presence of salt

(NaCl) along with the  $\text{Ga}_2\text{Al}_{18}$  crystallites. Due to high solubility of the crystallites, only minimal washing with methanol was attempted, so additional salt was likely present in the sample. Major peaks at 370, 393, 470 and 476  $m/z$  corresponded to Al(III) fragments. Larger fragments at 782 have isotope splitting patterns that must contain two M+2 isotopes, such as Cl ( $^{35}\text{Cl}$  and  $^{37}\text{Cl}$ ) and Ga ( $^{69}\text{Ga}$  and  $^{71}\text{Ga}$ ). Similar results were observed in the hydrolyzed solution although additional larger fragments were observed at 1308 and 1657  $m/z$  that also contain isotope splitting that is indicative of the presence of both gallium and chlorine. Significant more noise was also observed in the solution data due to the presence of sodium and chlorine ions.

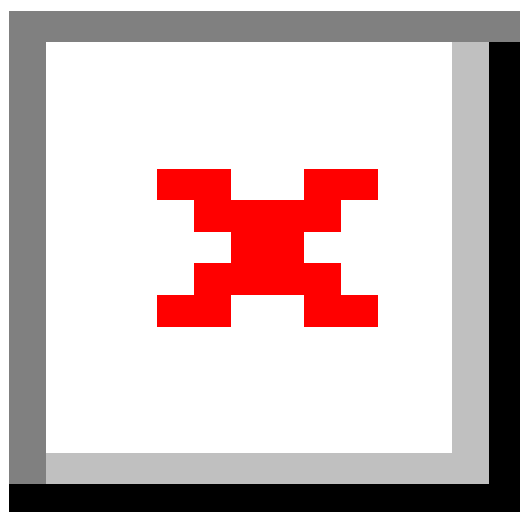


**Figure S3.** ESI-MS for the  $\text{Ga}_2\text{Al}_{18}$  crystals dissolved in water.

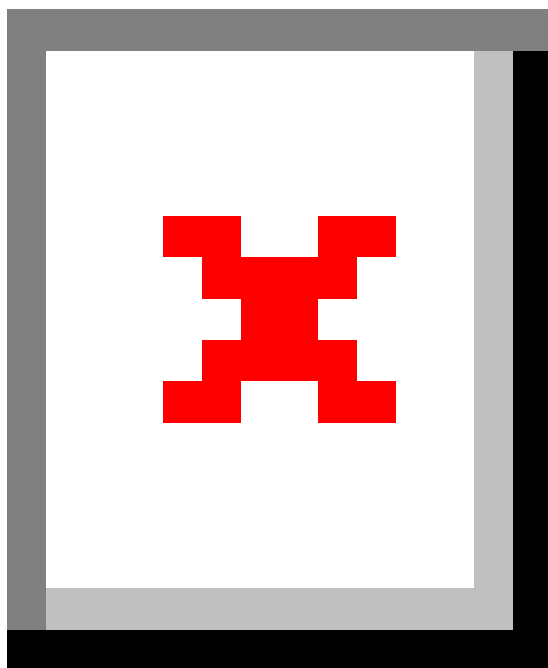
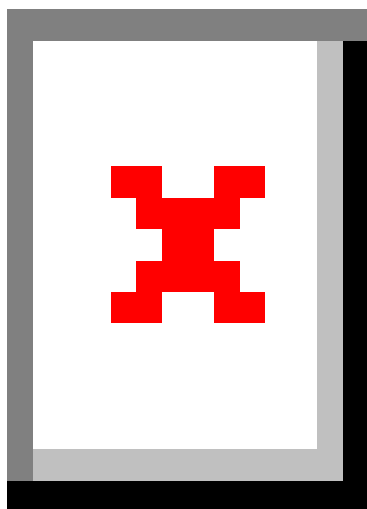


**Figure S4.** ESI-MS for the hydrolyzed solution that resulted in the formation of the  $\text{Ga}_2\text{Al}_{18}$  clusters.

(a)



(b)

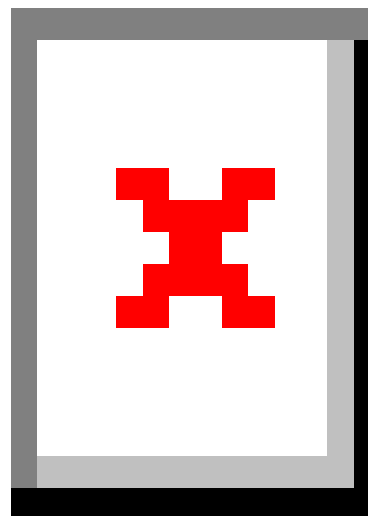


**Figure S5.** Expanded spectra of  $m/z$  peaks that indicate just the presence of (a) one M+2 isotope (Cl) or (b) two M+2 isotopes (Ga and Cl).

**Table S3.** ESI-MS data for the dissolved Ga<sub>2</sub>Al<sub>18</sub> crystals and the hydrolyzed solution that resulted in the formation of the Ga<sub>2</sub>Al<sub>18</sub> clusters. The major m/z peaks are assigned from the expanded spectra (example Fig. 4) to provide higher quality positions and possible fragment assignments listed below. The major fragments (>50%) for the hydrolyzed solutions are assigned along with minor fragments that contain obvious splitting patterns due to the presence of Ga and Cl isotopes.

<b>Dissolved Ga<sub>2</sub>Al<sub>18</sub></b>	<b>Hydrolyzed Ga/Al Solution</b>
m/z = 371 [Al <sub>6</sub> O <sub>2</sub> (OH) <sub>10</sub> (H <sub>2</sub> O) <sub>17</sub> ] <sup>4+</sup> +2 Cl <sup>-</sup>	m/z = 371 [Al <sub>6</sub> O <sub>2</sub> (OH) <sub>10</sub> (H <sub>2</sub> O) <sub>17</sub> ] <sup>4+</sup> +2 Cl <sup>-</sup>
m/z = 393 [Al <sub>11</sub> O <sub>4</sub> (OH) <sub>21</sub> ] <sup>4+</sup> + 2 Cl <sup>-</sup>	m/z = 393 [Al <sub>11</sub> O <sub>4</sub> (OH) <sub>21</sub> ] <sup>4+</sup> + 2 Cl <sup>-</sup>
m/z = 470 [Al <sub>13</sub> O <sub>6</sub> (OH) <sub>23</sub> (H <sub>2</sub> O) <sub>2</sub> ] <sup>4+</sup> + 2 Cl <sup>-</sup>	m/z = 518 [GaAl <sub>8</sub> O <sub>4</sub> (OH) <sub>12</sub> (H <sub>2</sub> O) <sub>17</sub> ] <sup>7+</sup> + 5 Cl <sup>-</sup>
m/z = 476 [Al <sub>12</sub> O <sub>5</sub> (OH) <sub>22</sub> (H <sub>2</sub> O) <sub>6</sub> ] + 2 Cl <sup>-</sup>	m/z = 783 [GaAl <sub>4</sub> (OH) <sub>7</sub> (H <sub>2</sub> O) <sub>10</sub> ] <sup>8+</sup> + Na <sup>+</sup> + 8 Cl <sup>-</sup>
m/z = 783 [GaAl <sub>4</sub> (OH) <sub>7</sub> (H <sub>2</sub> O) <sub>10</sub> ] + Na <sup>+</sup> + 8 Cl <sup>-</sup>	m/z = 1308 [GaAl <sub>5</sub> (OH) <sub>4</sub> (H <sub>2</sub> O) <sub>32</sub> ] <sup>+</sup> + 13 Cl <sup>-</sup>
	m/z = 1658 [Ga <sub>2</sub> Al <sub>18</sub> (OH) <sub>32</sub> (H <sub>2</sub> O) <sub>68</sub> ] <sup>2+</sup> + 26 Cl <sup>-</sup>

## **DFT Calculations**

### **Computational method details – Ga<sub>2</sub>Al<sub>18</sub> and Al<sub>2</sub>Al<sub>18</sub>**

Periodic density functional theory (DFT) calculations were performed as implemented in the DMol<sup>3</sup> code developed by Delley<sup>13</sup> using the generalized gradient approximation (GGA) of Perdew, Burke, and Ernzerhof (PBE),<sup>22</sup> and a 2×2×2 Monkhorst-Pack (MP) *k*-point grid. The calculations use a double numerical plus polarization basis set (DNP), with a real-space cutoff,  $r_{\text{cut}}$ , of 3.5 Å. **Ga<sub>2</sub>Al<sub>18</sub>** ([Ga<sub>2</sub>Al<sub>18</sub>O<sub>8</sub>(OH)<sub>36</sub>(H<sub>2</sub>O)<sub>12</sub>]<sup>8+</sup>) atomic positions were fully relaxed within the cell which was modeled at the experimentally determined lattice parameters. As detailed in the main text, the counter ions were modeled by replacing the sulfonate groups of 2,7-NDS with sulfate groups, similar to as was done in our study of Cu<sub>2</sub>Al<sub>30</sub>.<sup>6</sup> The Al<sub>2</sub>Al<sub>18</sub> ([Al<sub>2</sub>Al<sub>18</sub>O<sub>8</sub>(OH)<sub>36</sub>(H<sub>2</sub>O)<sub>12</sub>]<sup>8+</sup>) analogue was modeled in the same cell geometry, again allowing

for full optimization of the atomic positions within the cell. We refer to these cluster geometries collectively as  $M_2Al_{18}$ , where  $M=Al$  or Ga.

### GaAl<sub>12</sub> and Al<sub>13</sub> calculations

In addition to DFT calculations of the  $M_2Al_{18}$  species, periodic calculations of  $\delta$ -MAI<sub>12</sub> (Na- $\delta$ -[MAI<sub>12</sub>O<sub>4</sub>(OH)<sub>24</sub>(H<sub>2</sub>O)<sub>12</sub>][SO<sub>4</sub>]<sub>4</sub>·19H<sub>2</sub>O) and  $\epsilon$ -MAI<sub>12</sub> ( $\epsilon$ -[MAI<sub>12</sub>O<sub>4</sub>(OH)<sub>24</sub>(H<sub>2</sub>O)<sub>12</sub>][SO<sub>4</sub>]<sub>3</sub>·16H<sub>2</sub>O, two formula weights are in one unit cell) were also performed. The Keggin geometries were based on the crystal structures of  $\delta$ -Al<sub>13</sub> and  $\epsilon$ -Al<sub>13</sub> reported by Rowsell<sup>23</sup> and Johansson,<sup>24</sup> shown in Figure S6. The Ga Keggin structures were modeled by substituting Ga into the tetrahedral position from the Al Keggin structures. The basis set cutoff radius was tested by monitoring the tetrahedral  $M$ -O bond length as summarized in Table S4 for the  $\epsilon$ -MAI<sub>12</sub> structures. In order to efficiently optimize the coordinates in the initial  $\epsilon$ - and  $\delta$ -MAI<sub>12</sub> structures, the positions of the oxygen atoms in the water molecules were constrained, while all other coordinates of the structures were fully relaxed. In all cases, the angles of the experimental crystal structures were used, while the lattice constants and atomic positions were optimized. The lattice constants of the tridecamer Al and Ga species were optimized at the DFT level using a  $2\times 2\times 2$  Monkhorst-Pack (MP)  $k$ -point grid and a real-space cutoff,  $r_{\text{cut}}$ , of 4.0 Å. For the two  $\epsilon$ -MAI<sub>12</sub> species, the optimized bulk lattice constants for both were determined to be (with percent error from the experimental  $\epsilon$ -Al<sub>13</sub> structure in parentheses)  $a = 14.1800$  Å (0.0%),  $b = 11.5000$  Å (0.0%), and  $c = 18.0846$  Å (+2.0%).<sup>24</sup> The results of the lattice constants for the  $\delta$ -MAI<sub>12</sub> species are  $a = 13.8153$  Å (-2.0%),  $b = 15.0402$  Å (0.0%), and  $c = 16.1857$  Å (+2.0%), where again the comparison to the experimental values are given in parentheses.<sup>23</sup>

**Table S4.** Tetrahedral  $M$ -O bond distances as a function of DNP basis set  $r_{\text{cut}}$  for the  $\epsilon$ - $MA_{12}$  Keggin structures.

$r_{\text{cut}}$ (Å)	$\epsilon$ - $Al_{13}$	$\epsilon$ - $GaAl_{12}$
3.50	1.856	1.925
3.75	1.856	1.926
4.00	1.858	1.926
4.25	1.857	1.928
4.50	1.856	1.927
4.75	1.856	1.925

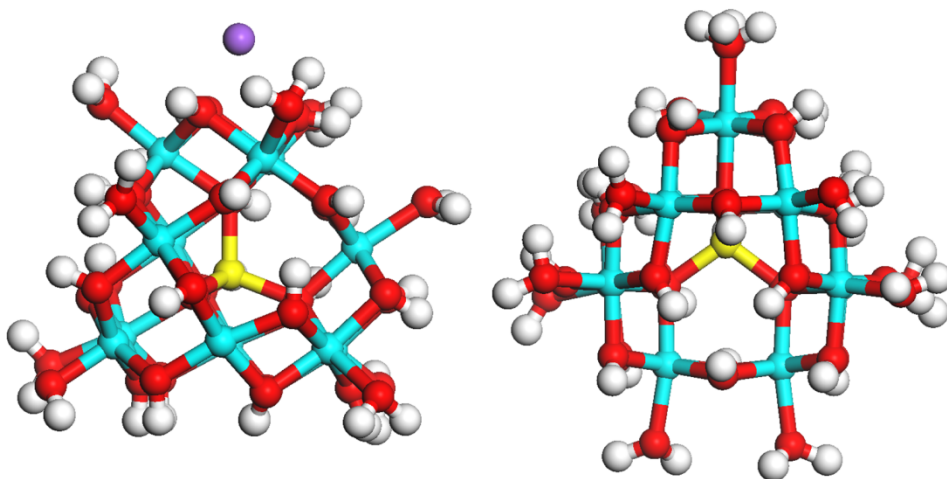


**Figure S6.** Ball and stick representation of DFT models of the  $\delta$  (left) and  $\epsilon$  (right) Keggin structures. The tetrahedral cations are shaded yellow and can be Al or Ga. Aluminum, oxygen, hydrogen, and sodium are shown in blue, red, white, and purple, respectively.

Optimized bond distances from the tetrahedral  $M$  atom to the oxygen for the Keggin structures are tabulated and compared to the experimental structures in Table S5 for  $\epsilon$ - $MA_{12}$  and Table S6 for the  $\delta$ - $MA_{12}$  species. Table S5 also contains the bond distances from the  $\epsilon$ - $GaAl_{12}$  experimental structure from Parker *et al.*<sup>8</sup> There is excellent structural agreement between the theoretical and experimental structures, where available.

**Table S5.** Details of the experimental and theoretical  $\epsilon$ - $MAI_{12}$  Keggin geometries in terms of the tetrahedral  $M$ -O distances. The numbers in parentheses are the percent differences between the DFT results and the corresponding experimental  $\epsilon$ - $Al_{13}$  structure.

(Å)	$\epsilon$ - $Al_{13}$ crystal <sup>24</sup>	$\epsilon$ - $GaAl_{12}$ crystal <sup>7</sup>	DFT Model $\epsilon$ - $Al_{13}$	DFT Model $\epsilon$ - $GaAl_{12}$
$M-O_1$	1.844	1.878	1.879 (1.90)	1.950
$M-O_2$	1.843	1.878	1.842 (-0.054)	1.908
$M-O_3$	1.837	1.878	1.841 (0.22)	1.916
$M-O_4$	1.845	1.878	1.877 (1.73)	1.940

**Table S6.** Details of the experimental and theoretical  $\delta$ - $MAI_{12}$  Keggin geometries in terms of the tetrahedral  $M$ -O distances. The numbers in parentheses are the percent differences between the DFT results and the corresponding experimental  $\delta$ - $Al_{13}$  structure.

(Å)	$\delta$ - $Al_{13}$ Crystal <sup>23</sup>	DFT Model $\delta$ - $Al_{13}$	DFT Model $\delta$ - $GaAl_{12}$
$M-O_1$	1.821	1.845 (1.32)	1.919
$M-O_2$	1.788	1.800 (0.67)	1.867
$M-O_3$	1.798	1.811 (0.72)	1.877
$M-O_4$	1.790	1.792 (0.11)	1.867

### Computational methods benchmarking

We carry out benchmarking of our computational methods compared to the level of theory used in other theoretical studies of Keggin clusters. In recent work by Reusser *et al.*,<sup>12</sup>  $\epsilon$ - $MAI_{12}$  Keggin molecules with different heteroatom substitutions were modeled using Gaussian 09<sup>25</sup> with the 6-31G\* basis set, the B3LYP<sup>26</sup> exchange correlation functional, and with the polarizable continuum model (PCM)<sup>25</sup> to account for aqueous effects. In comparing the basis sets used in this study with that used by Reusser and co-workers, we note that they are comparable, and it is reported that DNP is more accurate than a like-sized Gaussian basis set.<sup>27</sup> Broadly speaking, the consensus in the literature is that the B3LYP functional is acceptable for calculating various properties of different chemical systems, and outperforms other density functionals in some applications. However, hybrid functionals are computationally demanding,

and therefore it is desirable to use a local functional in cases where similar results can be obtained. We therefore carry out tests to assess the dependence of structural and energetic results for  $\epsilon$ - $MAI_{12}$  Keggin on the choice of exchange-correlation functional. As only local density functionals are available in the DMol<sup>3</sup> software, Gaussian 09 calculations are used to compare the PBE and B3LYP functional performance. We model the  $\epsilon$ - $MAI_{12}$  Keggin with  $M$ =Ga, Al, or Ge as isolated molecules using PCM. Finally, to provide a more direct comparison to the DMol<sup>3</sup> methods, we carry out molecular calculations in DMol<sup>3</sup> using the same basis set and exchange-correlation functional as in our periodic calculations (DNP/PBE), and with the addition of the conductor-like screening model (COSMO) to account for aqueous effects.<sup>28</sup> Reviews about continuum solvent models have concluded that the differences in COSMO and PCM are negligible.<sup>29</sup> Both COSMO and PCM model a continuous surface charge around the system and both model the medium surrounding the system as a conductor.<sup>29</sup>

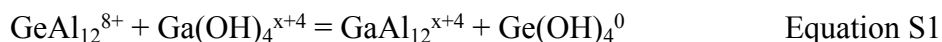
The results for the average tetrahedral  $M$ -O bond distances are reported in Table S7 for the different computational methods. We also include the experimental values, which are based on the solid crystal structure. As a point of reference, the parenthetical values next to the theoretical values report the percent error compared to the reported crystal structure. We note that all three methods show  $M$ -O distances that are systematically longer than the experimental distances, which may be due to differences in molecular and solid geometries. Similar  $M$ -O distances are achieved for all methods for each of the three Keggin, and thus there is no clear advantage to any of the methods based on structural results.

As an energy benchmark of the three computational methods, we follow after Reusser and co-workers and use Equation S1 to calculate the formation energy of  $\epsilon$ - $GaAl_{12}$ . The values obtained are -2.13 eV, -2.23 eV, and -2.31 eV for the PBE/COSMO, B3LYP/PCM, and

PBE/PCM methods, respectively. The range of 0.18 eV (4.15 kcal/mol) is within reasonable chemical accuracy achievable by DFT, and thus we conclude that the choice of computational methods used in this study are appropriate.

**Table S7.** Details of the theoretical molecular  $\epsilon$ - $MAl_{12}$  Keggin geometries in terms of the average tetrahedral  $M$ -O distances for different computational methods. The experimental results for the M-O distances in the crystal structure are also given. The values in parentheses give the percent error compared to experiment.

(Å)	Experimental Values	DMol <sup>3</sup> PBE/COSMO	Gaussian 09 B3LYP/PCM	Gaussian 09 PBE/PCM
$\epsilon$ -Al <sub>13</sub>	1.83 <sup>7</sup>	1.815(1.25)	1.813(1.36)	1.823(0.82)
$\epsilon$ -GaAl <sub>12</sub>	1.88 <sup>8</sup>	1.882(0.32)	1.875(0.69)	1.881(0.37)
$\epsilon$ -GeAl <sub>12</sub>	1.82 <sup>29</sup>	1.810(0.71)	1.790(1.80)	1.802(1.14)



### Additional Ga<sub>2</sub>Al<sub>18</sub> and Al<sub>2</sub>Al<sub>18</sub> Computational Results

Details of the optimized Ga<sub>2</sub>Al<sub>18</sub> and Al<sub>2</sub>Al<sub>18</sub> cluster geometries are given in Table S8. Compared to the experimental Ga-O bond lengths that range from 1.858 to 1.898 Å the theoretical distances are 1.898 to 1.933 Å. The DFT overestimation of Ga-O bond distances by 1.26-2.15% is consistent with results of other DFT studies on corundum Ga<sub>2</sub>O<sub>3</sub>.<sup>30</sup> As noted in the article text, the experimental structure shows elongation of the Al3-O2 and Al12-O14 bond to be 2.087(3) Å. In the DFT models we also see elongation of these bonds, with a distance of 2.098 Å, which is 0.5% longer than experiment.

In comparing Al and Ga, it is intuitive to consider how the larger ionic radius of Ga impacts the  $M_2Al_{18}$  structure. To this end, we compare  $r_{\text{Otet-Aloct}}$ , the bond distances between the oxygen atoms in the tetrahedral Al/Ga sites and octahedral Al. As shown in Table S8, the tetrahedral Ga-O distances are longer than the tetrahedral Al-O distances by 0.066 – 0.070 Å. Since each tetrahedral site oxygen is also coordinated to three octahedral Al centers, the Ga-O

elongation is compensated by relatively small (0.030 Å on average) contractions of  $r_{\text{Otet-Aloct}}$ . We can also make this comparison between the  $\epsilon$ - $M\text{Al}_{12}$  structures and we see once again relatively small (0.020 Å on average) contractions of  $r_{\text{Otet-Aloct}}$ .

**Table S8.** Details of the experimental  $\text{Ga}_2\text{Al}_{18}$  and theoretical  $\text{Ga}_2\text{Al}_{18}$  and  $\text{Al}_2\text{Al}_{20}$  geometries in terms of the tetrahedral  $M$ -O and distance between the two tetrahedral  $M$  atoms,  $M\text{---}M$ .

(Å)	$\text{Ga}_2\text{Al}_{18}$ Crystal	DFT Model $\text{Ga}_2\text{Al}_{18}$	DFT Model $\text{Al}_2\text{Al}_{18}$
$M\text{---}M$	3.575	3.620	3.594
$M\text{-O}_1$	1.858	1.898	1.829
$M\text{-O}_2$	1.898	1.926	1.860
$M\text{-O}_3$	1.888	1.922	1.852
$M\text{-O}_4$	1.895	1.933	1.860

The electronic structure of the Ga/Al  $\epsilon$ -Keggin and  $\text{Ga}_2\text{Al}_{18}/\text{Al}_2\text{Al}_{18}$  structures is studied and compared to probe whether differences in the tetrahedral cation give rise to different bonding interactions in the structures. Mulliken population analysis of Ga/Al in the  $M_2\text{Al}_{18}$  clusters are 1.34 and 1.41 e, respectively, while in the  $\epsilon$ -Keggin the values are 1.32 and 1.41 e, respectively. Atom-projected density of states (PDOS) analysis offers a qualitative means of studying the bonding interactions in material in terms of chemically intuitive atomic orbitals. For example, covalent interactions are characterized by PDOS intensity for different states at the same energies, delocalization is reflected in the width of PDOS intensity, and ionization is related to the relative PDOS intensity below and above the Fermi level. The PDOS for the  $\epsilon$ - $M\text{Al}_{12}$  species are in Figure S7. For both epsilon Keggin, there are broad regions of overlap between the Al/Ga  $p$  and  $d$  states and the O  $p$  states in the range of -1 to -5 eV. The density of states projected onto the Al/Ga  $d$  states also shows intensity in this region, with similar shape and magnitude to that of the  $p$  states. Al and Ga  $s$  states exhibit more localized interaction with O  $p$ , with common intensities (which are larger in Ga) noted near -7.2 eV and -5.2 eV in both.

The PDOS of the  $M_2Al_{18}$  clusters are shown in Figure 3, and are described in the primary text of the article. The PDOS for the  $\epsilon$ -Keggin and  $M_2Al_{18}$  clusters are strikingly similar, and in both structures the Al/Ga analogues exhibit electronic structure with similar salient features. Not shown, but also investigated, is the PDOS of octahedral Al and particle surface O atoms, which are also found to be similar as a function of cluster structure and tetrahedral cation identity. Since Ga substitution of the Keggin tridecamer species is known to occur, we interpret the similar electronic structure for the two structures with heteroatom substitution to be indicative that the Ga in the  $Ga_2Al_{18}$  cluster does not provide any unique stability relative to Al, and that the pure Al form may also be stable.

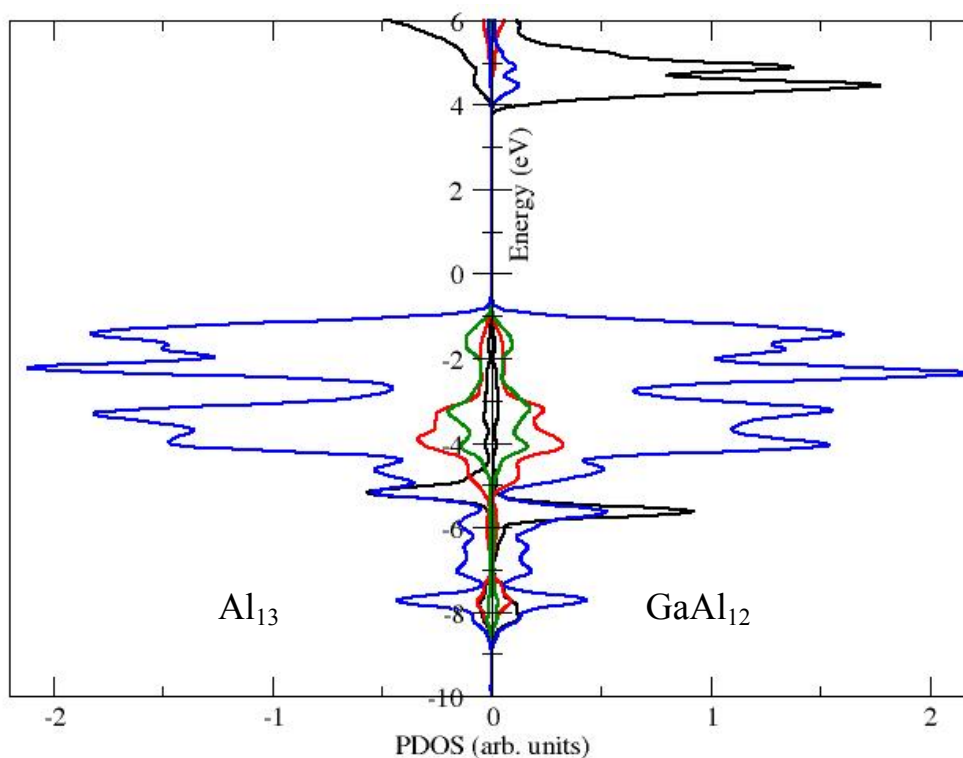


**Figure S7.** PDOS for  $\epsilon$ - $MAAl_{12}$ . The PDOS intensities for  $Al_{13}$  are shown along the negative  $x$  direction while those for  $GaAl_{12}$  are along the positive  $x$  direction. The Fermi level is set to  $y=0$ . In each graph the  $M$ - $s$  projection is shown in black, the  $M$ - $p$  projection is shown in red, the  $M$ - $d$  projection is shown in green, and the  $O$ - $p$  projection is shown in blue.

## REFERENCES

- (14) Hoft, R. W. W. *COLLECT*, Delft, The Netherlands, 1998.
- (15) Sheldrick, G. M. *APEX II*, Bruker AXS: Madison, WI, 1996.
- (16) Sheldrick, G. M., *Acta Crystallographica Section A: Foundations of Crystallography* **2008**, *64*, 112-122.
- (17) Brese, N. E.; O'Keefe, M. *Acta Crstyallographica Section B* **1991**, *B47*, 192-197.
- (18) Bradley, S. M.; Kiddy, R. A.; Fyfe, C. A. *Inorg. Chem.* **1992**, *31* 1181-1185.
- (19) Akitt, J. W.; Greenwood, N. N.; Khandelwal, B.L; Lester, G. D. *J. Chem. Soc.-Dalton Trans.* **1972**, *5*, 604-610.
- (20) Fu, G.; Nazar, L. F.; Bain, A. D., *Chem..Mater.* **1991**, *3*, 602-610.
- (21) Harris, R. K.; Becker, E.D.; Cabral de Menezes, S. M.; Goodfellow, R; Granger, P. *Pure Appl. Chem.* **2001**, *73*, 1795–1818.
- (22) Perdew, J. P.; Burke, K.; Ernzerhof, M. *Phys. Rev. Lett.* **1996**, *77*, 3865-3868.
- (23) Rowsell, J.; Nazar, L. F. *J. Am. Chem. Soc.* **2000**, *122*, 3777-3778.
- (24) Johansson, G. *Acta Chem. Scand.* **1960**, *14*, 771-773.
- (25) Frisch, M. J.; Trucks, G. W.; Schlegel, H. B.; Scuseria, G. E.; Robb, M. A.; Cheeseman, J. R.; Scalmani, G.; Barone, V.; Mennucci, B.; Petersson, G. A.; and others. *Computer program: Gaussian 09, Revision B. 01*, Wallingford, Connecticut, 2009.
- (26) Becke, A. D. *J. Chem. Phys.* **1993**, 1372-1377.
- (27) Inada, Y.; Orita, H. *J. Comput. Chem.* **2008**, *29*, 225-232.
- (28) Klamt, A.; Schuurmann, G. *J. Chem. Soc. Perk. Trans.* **1993**, 799-805.
- (29) (a) Cramer, C. J.; Truhlar, D.G. *Chem. Rev.* **1999**, *99*, 2161-2200, (b) Tomasi, J.; Mennucci, B.; Cammi, R. *Chem. Rev.* **2005**, *105*, 2999-3094.
- (30) (a) Zhou, X.; Hensen, E. J.; van Santen, R. A.; Li, C. *Chem. Eur. J.* **2014**, *20*, 6915–6926, (b) He, H.; Orlando, R.; Blanco, M.; Pandey, R.; Amzallag, E.; Baraille, I.; Rérat, M. *Phys. Rev. B.* **2006**, *74*, 195123-195128.